

# Onset of Antiferromagnetism in $\text{UPt}_3$ via Th-substitution: A Muon Spin Spectroscopy Study

M. J. Graf<sup>a</sup>, A. de Visser<sup>b</sup>, C. P. Opeil<sup>a</sup>, J. C. Cooley<sup>c</sup>, J. L. Smith<sup>c</sup>, A. Amato<sup>d</sup>,  
C. Baines<sup>d</sup>, F. Gygax<sup>e</sup>, and A. Schenck<sup>e</sup>

a - Department of Physics, Boston College, Chestnut Hill, MA 02467

b - Van der Waals - Zeeman Institute, University of Amsterdam, 1018 XE Amsterdam, The Netherlands

c - Los Alamos National Laboratory, Los Alamos, NM 87545

d - Paul Scherrer Institute, CH-5232 Villigen, Switzerland

e - Institute for Particle Physics of ETH Zürich, PSI CH-5232 Villigen, Switzerland

PACS numbers: 71.27.+a, 74.70.Tx, 75.30.Kz, 76.75.+i

## Abstract

Muon-spin spectroscopy has been used to study in detail the onset of large-moment antiferromagnetism (LMAF) in  $\text{UPt}_3$  as induced by Th substitution. We have studied  $\text{U}_{1-x}\text{Th}_x\text{Pt}_3$  for  $0 \leq x < 0.05$  and find that the two-component depolarization function used to characterize the muon response in Pd-induced LMAF is also applicable to  $(\text{U,Th})\text{Pt}_3$ . However, the transition into the antiferromagnetic phase, as the temperature is lowered, is much broader for Th substitution than for Pd substitution, making it difficult to detail the competition between superconductivity and LMAF in  $(\text{U,Th})\text{Pt}_3$ . The broadening may be a result of the effects of disorder on the time fluctuations associated with anomalous small-moment antiferromagnetism.

## 1. Introduction

### *a. UPt<sub>3</sub> and U(Pt,Pd)<sub>3</sub>*

The compound UPt<sub>3</sub> is an exemplary unconventional superconductor.<sup>1</sup> Superconductivity emerges at  $T_c \approx 0.5$  K from a strongly correlated heavy-fermion state that also exhibits an anomalous form of antiferromagnetism ("small-moment" antiferromagnetism, or SMAF) below about 6 K.<sup>2</sup> This superconducting state has a striking double transition<sup>3</sup> and multiple superconducting phases in applied magnetic fields.<sup>4</sup> A vast amount of experimental and theoretical work has been devoted to describing this superconducting state. Experimentally, it is known that the magnetic SMAF couples to the superconducting state,<sup>5,6</sup> as expected for magnetically-mediated pairing. Knight shift<sup>7</sup> and substitutional studies<sup>8,9</sup> indicate that the superconducting state has odd parity. These experimental results are well accounted for by phenomenological Ginzburg-Landau theories, which have complex 1D or 2D order parameters, and for which some intrinsic symmetry-breaking field lifts internal degeneracies and results in the split superconducting transition.<sup>1</sup> Pressure<sup>10</sup> and substitutional<sup>11</sup> studies indicate that the anomalous SMAF state is the symmetry-breaking field, although lattice distortions and defects<sup>12-14</sup> are possible alternatives.

While it is generally accepted that the pairing is due to magnetic correlations, the magnetic state from which superconductivity emerges is poorly understood. Neutron and magnetic x-ray scattering clearly signal a transition into the SMAF.<sup>2,6</sup> Additional Bragg scattering peaks appear at 6K that indicate antiferromagnetic ordering in the basal plane of this hexagonal closed packed-like system. The order parameter exhibits an anomalous, quasi-linear temperature dependence. Bulk thermodynamic signatures of this phase are expected to be difficult to observe due to the small size of the ordered moment ( $0.02 \mu_B$  as  $T \rightarrow 0$  K), but sufficiently sensitive local probes such as NMR<sup>15</sup> and muon spin relaxation/rotation ( $\mu$ SR)<sup>16,17</sup> also do not signal a transition into the SMAF state. Thus it has been suggested that in UPt<sub>3</sub>, SMAF is not a statically ordered phase. Rather, it fluctuates on time scales that are short compared to the typical NMR and  $\mu$ SR time scales (down to  $10^{-9}$  s), yet they are long compared to the nearly-instantaneous scales ( $< 10^{-11}$  s) of neutron and x-ray scattering.<sup>18</sup> This picture qualitatively explains the discrepancy between the neutron measurements and  $\mu$ SR and NMR data. A similar picture has recently been proposed for the high-temperature superconductor YBa<sub>2</sub>Cu<sub>3</sub>O<sub>6.5</sub>.<sup>19</sup> However, to date there is no plausible

model describing how macroscopically large volumes of magnetic order fluctuate so rapidly nor how such a fluctuating state can act as a symmetry-breaking field for the superconducting phase.

By doping  $\text{UPt}_3$  with Pd, a conventional AFM phase is induced, which competes with superconductivity. Neutron scattering<sup>20,21</sup> and  $\mu\text{SR}$ <sup>17</sup> measurements signal a transition into a spin-density wave antiferromagnetic state for  $\text{U}(\text{Pt}_{1-x}\text{Pd}_x)_3$  for  $0.01 \leq x \leq 0.10$ , with the zero-temperature staggered moment and Néel temperature reaching maxima of  $0.63 \mu_B$  and 6.2 K, respectively, when  $x = 0.05$ . In contrast to the SMAF state, NMR<sup>22</sup> and thermodynamic<sup>23,24</sup> measurements clearly detect the antiferromagnetic ordering for  $x \geq 0.02$ . This conventionally ordered state is termed the "large-moment" antiferromagnetic phase (LMAF). The LMAF phase has the same magnetic structure as the SMAF, suggesting that the LMAF phase and the anomalous SMAF are closely related. More recently, the LMAF transition temperatures have been tracked with decreasing Pd concentration via  $\mu\text{SR}$ <sup>25</sup> down to  $T_N = 0.45$  K for  $x = 0.007$ ;  $T_N$  extrapolates to 0 K at  $x_{c,AFM} \approx 0.006$ . Interestingly, for concentrations lower than this the superconducting transition temperature  $T_c$  becomes non-zero, i.e. the critical concentration for suppression of superconductivity,  $x_{c,SC}$ , is approximately equal to the critical concentration for the onset of LMAF, demonstrating that static antiferromagnetism and odd-parity superconductivity are incompatible in this system. These results are summarized in the magnetic/superconducting phase diagram in Fig. 1.

The fact that  $x_{c,SC} \approx x_{c,AFM}$  appears to be related to strong magnetic fluctuations in the vicinity of a quantum critical point. It was proposed that an increase in the spectral weight of antiferromagnetic fluctuations relative to that for ferromagnetic (FM) fluctuations would drive  $T_c$  to 0 K if pairing were mediated by FM fluctuations.<sup>25</sup> This scenario is appealing, as the qualitative expectation is that odd-parity superconductivity is most effectively mediated by FM fluctuations. Alternately, the suppression of  $T_c$  to 0 K may be a consequence of strong inelastic scattering near  $x_{c,AFM}$ .<sup>26</sup> In either case, it is clear that understanding the onset of LMAF will play a key role in detailing the nature of the unconventional superconducting state in  $\text{UPt}_3$ .

### *b. Review of previous $\mu\text{SR}$ studies of the LMAF in $\text{U}(\text{Pt},\text{Pd})_3$*

The goal of this work is to probe the onset of magnetism in  $(\text{U,Th})\text{Pt}_3$  using  $\mu\text{SR}$ , and so first previous results from  $\mu\text{SR}$  studies of  $\text{U}(\text{Pt},\text{Pd})_3$  will be reviewed. Zero-magnetic-field  $\mu\text{SR}$

is a local probe measurement of the magnetic field at the muon stopping site(s) in the sample.<sup>27</sup> If the implanted polarized muons are subject to magnetic interactions, their polarization becomes time dependent ( $\mathbf{P}_\mu(t)$ ). By measuring the asymmetric distribution of positrons emitted when the muons decay as a function of time, the time evolution of  $\mathbf{P}_\mu(t)$  can be deduced. The function  $P_\mu(t)$  is defined as the projection of  $\mathbf{P}_\mu(t)$  along the direction of the initial polarization:  $P_\mu(t) = \mathbf{P}_\mu(t) \cdot \mathbf{P}_\mu(0) / P_\mu(0) = G(t) P_\mu(0)$ . The depolarization function  $G(t)$  reflects the normalized muon-spin autocorrelation function  $G(t) = \langle \mathbf{S}(t) \cdot \mathbf{S}(0) \rangle / S(0)^2$ , which depends on the average value, distribution, and time evolution of the internal fields, and it therefore contains all the physics of the magnetic interactions of the muon inside the sample.

Experiments<sup>17</sup> on U(Pt,Pd)<sub>3</sub> in the LMAF phase ( $T \ll T_N$ ) show that the depolarization is best described by a two-component function:

$$G(t) = A_{osc} \left[ \frac{2}{3} \exp(-\lambda t) \cos(2\pi\nu t + \phi) + \frac{1}{3} \exp(-\lambda' t) \right] + A_{KL} G_{KL}(\lambda_{KL} t) . \quad (1)$$

The first term is the time-dependent depolarization function for a muon precessing with frequency  $\nu$  in a static, non-zero local magnetic field, and since the samples are polycrystalline, on average 1/3 of the muon spins are effectively aligned parallel to the field and thus have  $\nu = 0$ . The exponential decays  $\lambda$  and  $\lambda'$  reflect the distribution of local fields due to static variations and/or dynamical fluctuations. The second term is a Kubo-Lorentz decay

$$G_{KL}(\lambda_{KL} t) = \frac{1}{3} + \frac{2}{3} (1 - \lambda_{KL} t) \exp(-\lambda_{KL} t) . \quad (2)$$

In this case, depolarization with characteristic rate  $\lambda_{KL}$  is caused by an isotropic Lorentzian distribution of local fields with an average value of zero. The amplitudes of these two components are found to be equal,  $A_{osc} \approx A_{KL}$ .

The two-component response indicates that muons have two distinct stopping sites in the sample, and since  $A_{osc} \approx A_{KL}$ , they are equally likely to stop at either type of site. This can result from two distinct crystallographic locations where the muon comes to rest or from the sample having two different mesoscopic magnetic environments (i.e., magnetically inhomogeneous).<sup>28</sup>

Transverse magnetic field  $\mu$ SR studies of single-crystal  $\text{U}(\text{Pt}_{0.95}\text{Pd}_{0.05})_3$  indicate a single crystallographic stopping site and so support the latter interpretation.<sup>29</sup> Still, the origin of the two-component response remains an unresolved problem, and so the various parameters in Equations (1) and (2) are considered as phenomenological in nature.

For samples with  $T > T_N$ , the depolarization is found to result from the Gaussian distribution of static, randomly-oriented magnetic fields due to  $^{195}\text{Pt}$  nuclei. As expected, the form of the depolarization function is given by the Kubo-Toyabe function

$$G_{KT}(\Delta_{KT}t) = A_{KT} \left[ \frac{1}{3} + \frac{2}{3} (1 - \Delta_{KT}^2 t^2) \exp\left(-\frac{1}{2} \Delta_{KT}^2 t^2\right) \right], \quad (3)$$

with  $\Delta_{KT} \approx 0.07 \mu\text{s}^{-1}$ . There is no zero-field  $\mu$ SR signature for the SMAF state, so Eq. (3) works equally well in the paramagnetic phase or the anomalous SMAF region.

Finally, in the vicinity of the Néel transition, the muon ensemble will be sensitive to sample domains possessing slightly different transition temperatures. The total depolarization will therefore be given in this temperature range by a sum of Eqs. (1) and (3). The breadth of the transition from LMAF to paramagnetism (or SMAF) is manifest in the amplitude of the magnetic component  $A_M = A_{osc} + A_{KL}$  relative to the total signal,  $A_T = A_{MAG} + A_{NM}$ . The non-magnetic component  $A_{NM}$  is given by  $A_{KT}$ , and the total signal amplitude is assumed to be constant and so is fixed as a fitting constraint. Typical transition widths in  $\text{U}(\text{Pt},\text{Pd})_3$  are less than 1 K.

The possibility of magnetic inhomogeneity in  $\text{U}(\text{Pt}, \text{Pd})_3$ , as evidenced by the two-component depolarization function, is particularly interesting since it was recently discovered that  $\text{URu}_2\text{Si}_2$ , another U-based "small-moment" heavy fermion system is magnetically inhomogeneous. NMR measurements under applied pressure<sup>30</sup> showed that the small moment is caused by a small fraction of the sample volume having a relatively large local ordered moment, while the majority of the sample is paramagnetic. Neutron scattering yields an ordered moment that is averaged over the entire volume of the sample. While there are significant differences between the two systems, it is clearly of interest to further probe the possibility of magnetic inhomogeneity in  $\text{UPt}_3$  and  $\text{U}(\text{Pt},\text{Pd})_3$  with an eye to similarities with the  $\text{URu}_2\text{Si}_2$  system.

### *c. (U,Th)Pt<sub>3</sub>*

The goal of the present  $\mu$ SR study is to further investigate the nature of the LMAF phase, and its relationship to the SMAF phase, by inducing static antiferromagnetism in  $UPt_3$  by other means. Early neutron scattering,<sup>31</sup>  $\mu$ SR,<sup>32</sup> and magnetic, thermal, and transport measurements<sup>33</sup> on  $U_{1-x}Th_xPt_3$  showed that Th substitution also induces conventional antiferromagnetism in  $UPt_3$ , and it has the same magnetic structure as the LMAF phase in  $U(Pt,Pd)_3$ . Even though Th expands the crystallographic unit cell volume while Pd contracts it, both Pd and Th contract the  $c/a$  ratio, and so it appears that this is the relevant parameter controlling magnetic interactions.<sup>34,35</sup> However, these changes are very small, with a Th concentration of 0.1 producing a fractional change in  $c/a$  of  $7 \times 10^{-4}$ ,<sup>34</sup> and studies of other impurity substitutions cast some doubt on this conclusion.<sup>36</sup>

## **2. Samples, materials preparation and characterization**

Samples were prepared at Los Alamos National Laboratory from 99.99% pure U and Th, and 99.999% pure Pt. To ensure homogeneous mixing of the relatively small amounts of Th in the sample, U was melted into the starting amount of Th in several increments. The stoichiometrically appropriate amount of Pt was then melted into the U-Th alloy in 5-6 increments. This sample was melted 8-10 times, broken into small pieces, and then remelted another 8-10 times. The sample was then annealed in a high-vacuum furnace (base pressure  $6 \times 10^{-7}$  torr) at 850 ° C for 5 days, followed by a 2 day cooldown period. Finally, the samples were spark cut into  $6 \times 10 \times 1$  mm<sup>3</sup> plates which were polished for  $\mu$ SR measurements, and additional smaller bars were cut for characterization via resistive measurements, x-ray analysis, etc.

The resistance was measured using a four-terminal ac technique in a <sup>3</sup>He refrigerator. The residual resistivities  $\rho_0$  were determined by extrapolating the data between 1 K and 0.3 K (or above  $T_c$  for the samples with  $x = 0$  and 0.002) to 0 K assuming a power-law temperature dependence.<sup>37</sup>  $\rho_0$  varies smoothly across the series (see Fig. 2), indicating proper quality of the samples, and the increase is non-linear above roughly  $x = 0.005$ . This behavior was also observed for  $U(Pt,Pd)_3$ ,<sup>21,35</sup> and is believed to result from the opening of a gap at the Fermi surface upon formation of the LMAF spin-density wave state.<sup>33</sup>

The samples with  $x = 0$  and 0.002 were found to have superconducting transition temperatures of 0.55 K and 0.43 K, respectively, consistent with earlier results.<sup>38</sup> The  $x = 0.005$  sample is expected to have a  $T_c$  near 0.2 K. For samples with  $x = 0.02$  and 0.05 we observe broad resistive anomalies near 5 K and 7 K, respectively, associated with the onset of static antiferromagnetism (LMAF).<sup>33</sup> The  $x = 0.01$  sample has no resistive anomaly associated with magnetic ordering, but as shall be seen,  $\mu$ SR measurements clearly indicate AFM ordering at low temperatures. The lack of a resistive anomaly at  $T_N$  is similar to the case of  $x = 0.01$  in Pd-substituted UPt<sub>3</sub>.

### 3. $\mu$ SR Results for U<sub>1-x</sub>Th<sub>x</sub>Pt<sub>3</sub>

Muon-spin spectroscopy measurements on U<sub>1-x</sub>Th<sub>x</sub>Pt<sub>3</sub> were carried out on the  $\pi$ M3 beamline at the Paul Scherrer Institute in Villigen, Switzerland. Measurements were conducted between 1.7 K and 10 K using the General Purpose Spectrometer, and between 50 mK and 2.2 K using the Low Temperature Facility. Our primary results concern the muon-spin relaxation/rotation in zero applied magnetic field. The total depolarization amplitude (asymmetry) for each sample during a particular run was determined from measurements in a 100 G transverse magnetic field in the high-temperature paramagnetic state. In all the fitting procedures described below, the sum of the amplitudes of the fitting components is constrained to equal this total amplitude.

#### *a. $x \leq 0.002$*

As a consistency check with earlier works,<sup>16,17</sup> we measured the zero-field response of our  $x = 0$  sample. In the range from 2 K to 10 K the depolarization function is well-described by a Kubo-Toyabe fit, with  $\Delta_{KT} = 0.071(3) \mu\text{s}^{-1}$ , and no sign of entry into the anomalous SMAF phase was observed near 6 K. Results for the sample with  $x = 0.002$  were also fit by a Kubo-Toyabe equation, with  $\Delta_{KT} = 0.103(5) \mu\text{s}^{-1}$  independent of temperature over the limited range  $0.1 \text{ K} \leq T \leq 0.9 \text{ K}$ . This behavior is consistent with the results for pure UPt<sub>3</sub>. While  $\Delta_{KT}$  is slightly larger than for our pure sample, an additional measurement made at 7.3 K yielded  $\Delta_{KT} = 0.094(6) \mu\text{s}^{-1}$ . Therefore we rule out any weak increase of  $\Delta_{KT}$  as temperature is lowered and conclude that the sample remains non-magnetic at all temperatures studied.

These results are similar to observations made on  $\text{U}(\text{Pt}_{1-x}\text{Pd}_x)_3$  in the range  $0 \leq x \leq 0.005$ : the local muon response is unaffected by entry into the SMAF phase, and is primarily due to  $^{195}\text{Pt}$  nuclear moments.

*b.  $x \geq 0.006$*

For samples with  $0.006 \leq x \leq 0.05$ , we clearly observe the signature of static (on the typical muon timescale of  $10^{-9}$  s) AFM in our zero-field  $\mu\text{SR}$  results. At low temperatures ( $T \ll T_N$ ) all the data can be described by Eq. (1), and the parameters extracted are in close agreement with those reported<sup>17</sup> for  $\text{U}(\text{Pt},\text{Pd})_3$  within the LMAF phase. In Fig. 3 the low-temperature depolarization function versus time is shown for samples with  $x = 0.01, 0.02,$  and  $0.05$ . The spontaneous oscillation in the local magnetic field is clearly seen, but the damping increases strongly with decreasing Th concentration. Even at  $T = 40$  mK, the oscillation is barely discernible in the sample with  $x = 0.006$ . In Fig. 4 we plot the spontaneous oscillation frequency  $\nu$ , the oscillatory decay rates  $\lambda$  and  $\lambda'$ , and the Kubo-Lorentz  $\lambda_{KL}$  decay time as a function of Th concentration. For comparison, the values reported in Ref. 17 for  $\text{U}(\text{Pt}_{1-x}\text{Pd}_x)_3$  are shown, and the similarity in the values is evident.

The ratio of the oscillatory to the Kubo-Lorentz decay terms has been extracted from our fits to the data and is presented in Fig. 5 as a function of Th concentration. Within the statistical error of the fits, we find that  $A_{osc} = A_{KL}$  independent of thorium concentration, as was found for Pd-substituted samples. All these results indicate that the primary effect of these dopants is to perturb the magnetic interactions in the system and drive  $\text{UPt}_3$  to its magnetic instability; the type of impurity used to induce antiferromagnetic ordering does not significantly alter the ground state properties of the LMAF.

We now discuss our results for the temperature dependence. In order to fit our time-dependent curves as  $T$  increases towards  $T_N$ , we have incorporated the additional constraint that  $A_{osc} = A_{KL}$  (in addition to fixing the total amplitude), consistent with the procedure followed in Ref. 17 and with our experimental results at  $T \ll T_N$ . Also, we found that as  $T$  increases towards  $T_N$  use of Eq. (1) is not sufficient, and we have used the sum of Eqs. (1) and (3). The value of  $\Delta_{KT}$  was found for high temperature data ( $T > T_N$ ), and the resulting value is used as a

constant in the fitting procedure. This value falls in the  $0.05 - 0.08 \mu\text{s}^{-1}$  range for all the samples studied, apart from the previously mentioned  $x = 0.002$ .

Analysis of the  $x = 0.05$  data is straightforward. The two-component fit is found to work quite well except in a narrow region within about 1 K of the Néel temperature. It was found in Ref. 17 that the temperature dependence of the parameters  $\nu$  and  $\lambda_{KL}$  was mean-field-like, and could be fit to the form

$$P = P(0) \left[ 1 - \left( \frac{T}{T_N} \right)^\alpha \right]^\beta, \quad (4)$$

where  $T_N$  is the Néel temperature, and  $P$  is either  $\nu$  or  $\lambda_{KL}$ . The resulting temperature dependence of  $\nu$  and  $\lambda_{KL}$  is plotted for our  $x = 0.05$  sample in Figs. 6 and 7, respectively. Using Eq. (4) to fit the data yields  $T_N = 7.02(2)$  K for both curves;  $\nu(0) = 10.0(5)$  MHz,  $\alpha = 2.0(6)$ , and  $\beta = 0.42(5)$  from  $\nu(T)$ , and  $\lambda_{KL}(0) = 6.7(3) \mu\text{s}^{-1}$ ,  $\alpha = 3(1)$ , and  $\beta = 0.35(7)$  from  $\lambda_{KL}(T)$ . These values for the exponents compare favorably with those extracted in Ref. 17 for  $\text{U}(\text{Pt}_{0.95}\text{Pd}_{0.05})_3$ :  $\alpha = 2.1(3)$  and  $\beta = 0.39(2)$  from  $\nu(T)$ , and  $\alpha = 2.0(5)$  and  $\beta = 0.36(6)$  from  $\lambda_{KL}(T)$ . As pointed out in that work, the values are consistent with the theoretical prediction of  $\beta = 0.38$  derived for the 3D Heisenberg model<sup>39</sup> and  $\alpha = 2$  calculated for a cubic antiferromagnet.<sup>40</sup> We also note that our result for  $\nu(0)$  is in fair agreement with the value  $\nu(T=4.2\text{K}) = 8.0$  MHz observed by Heffner *et al.*<sup>32</sup> for  $\text{U}_{0.95}\text{Th}_{0.05}\text{Pt}_3$ .

A similar analysis for the temperature evolution of the muon response is problematic for samples with  $0.006 \leq x \leq 0.02$ . As seen in Fig. 4b, the decay  $\lambda$  increases dramatically with decreasing  $x$ . Moreover, the transition regions are quite broad and in the case of  $x = 0.01$  and  $0.02$  extend up to 7 K. The oscillatory behavior is highly damped at intermediate temperatures, and an accurate determination of the fitting parameters is quite difficult. Fitting the  $x = 0.02$  results for the temperature-dependent frequency below 4 K to Eq. (4) and using  $\alpha$  and  $\beta$  values of 2 and 0.38, respectively, we find a Néel temperature  $T_N = 5.05(5)$  K; the data and fit are shown in Fig. 6. A similar procedure for the  $x = 0.01$  sample yields a Néel temperature  $T_N = 3.50(5)$  K. The  $x = 0.05$  and  $x = 0.02$  mean-field  $T_N$  values are roughly consistent with early specific heat results for  $\text{U}_{0.9544}\text{Th}_{0.0456}\text{Pt}_3$  and  $\text{U}_{0.9801}\text{Th}_{0.0199}\text{Pt}_3$ .<sup>41</sup> In Ref. 32,  $\text{U}_{0.99}\text{Th}_{0.01}\text{Pt}_3$  was also studied via  $\mu\text{SR}$ , and no evidence of magnetic behavior was reported. However, it should be noted that the data for that sample were limited and extended only down to approximately 4 K.

The most striking aspect of the data is that our depolarization curves unambiguously show that magnetism is present in the system at temperatures well above the mean-field values for  $T_N$ . This is shown in Fig. 8, where the time-dependent polarization for  $x = 0.02$  is plotted over short times at temperatures of 5.3 K, 5.8 K, and 7.4 K, all of which are greater than the mean-field  $T_N$  of 5.05 K. While extraction of the exact parameters can be difficult when the condition  $T \ll T_N$  is no longer met, we can readily characterize the transition width by calculating the magnetic fraction of the total amplitude, i.e., the fraction of the total amplitude due to the depolarization described by Eq. (1). We have plotted this in Fig. 9 for samples with  $x = 0.01$ , 0.02, and 0.05. For comparison, we have also plotted the same quantity as extracted from the data of Ref. 17 for Pd-substituted samples. All the Pd-substituted samples have narrow transition widths, as does the Th-substituted sample with  $x = 0.05$ . However, the transitions for the Th-substituted samples with  $x = 0.01$  and 0.02 are quite broad and have a magnetic component up to  $T = 7$  K, which is the transition temperature for  $x = 0.05$ . It is clear that some form of magnetic inhomogeneity is present. A second sample with  $x = 0.02$ , independently fabricated at a later date, yields essentially identical data, confirming this behavior.

The validity of the assumption that  $A_{osc} = A_{KL}$ , and of the actual form of the fitting functions themselves, is debatable in the broad transition regions. However, the calculation of the fractional magnetic signal is insensitive to the functional form of the magnetic component. We have used a variety of different fitting functions to describe the magnetic contribution in the vicinity of  $T_N$ , and always reproduce the qualitative features shown in Figure 9.

*c.  $x = 0.005$*

We have also studied a sample with  $x = 0.005$ , which showed strong depolarization at low temperatures, but no oscillations were observed due to the heavy damping, as  $\lambda$  increases dramatically with decreasing Th concentration (see Fig. 4b). In order to follow the temperature dependence of the magnetism, Eq. (1) was modified by replacing the two oscillatory terms with two exponential decays (i.e., setting the frequency equal to zero). An analysis similar to the one presented in the preceding paragraph shows that once again the crossover from magnetic to non-magnetic behavior is quite broad, as shown in Fig. 10. It is important to note that for this sample the fractional magnetic signal reaches a maximum of about 0.6 at 85 mK, suggesting that the sample never has a fully formed LMAF state.

#### 4. Discussion

We conclude from the low-temperature ( $T \ll T_N$ ) results that the two-component response function (Eq. (1)) describes the depolarization within the LMAF phase whether induced by Pd or Th substitution, which show comparable values for the fit parameters and relative amplitudes of the different components. Thus it appears to be a general characteristic of the LMAF phase. The parameters  $\nu$  and  $\lambda_{KL}$ , which are representative of the internal field and internal field distribution for the two components, respectively, are somewhat larger in the Th-doped samples for a given value of  $x$ . Note that Th is far more effective in inducing the LMAF state, because in our notation, equal values of  $x$  translate into a number of Pd impurities which is three times the number Th impurities. This result is consistent with the assumption that the  $c/a$  ratio is the controlling factor in the onset of LMAF magnetism, since comparable values of  $x$  (in the notation used in this paper) are expected to produce comparable changes in  $c/a$ .<sup>42</sup> Magnetization data presented in Ref. 35 support this expectation.

The most striking difference between our data for Th-substituted samples and similar data for Pd-substituted samples is the very broad transition region from SMAF to LMAF, as shown in Fig. 9. X-ray diffraction analysis shows that there is less than 1% impurity phase in the samples, and it is known from earlier works that  $U_{1-x}Th_xPt_3$  remains single phase up to about  $x = 0.25$ .<sup>41</sup> Strong variations in the local Th concentration across the sample volume could conceivably produce the broad transitions, since the Néel temperature depends on  $x$ . Such an effect would be consistent with sharp transition observed for  $x = 0.05$  because the  $T_N(x)$  curve is expected to be fairly flat near  $x = 0.05$  (see Fig. 1), and so a given distribution of concentrations would produce a less-broad transition region. However, the transition regions for the  $x = 0.01$  and  $0.02$  samples extend up to 7 K. For the  $x = 0.01$  sample, we estimate that about 10 % of the sample volume would need to have a local Th concentration well above  $x = 0.02$  in order to reproduce the broadening shown in Fig. 9. This would severely deplete other regions, yet the data shown in Fig. 9 show that the sample has a negligible volume fraction with Néel temperature less than 2 K. Moreover, such dramatic inhomogeneity is inconsistent with smooth variation of the residual resistivity shown in Fig. 2. Thus chemical inhomogeneity seems unlikely to be the cause of the observed broadening.

An alternate explanation for the broadening of the SMAF-to-LMAF crossover involves the effect of Th disorder on the anomalous SMAF phase. If the SMAF phase is indeed a time-fluctuating version of the LMAF phase, then Th impurities may serve to slow down the fluctuations. When the fluctuation timescale becomes comparable to, or longer than, the typical muon spectroscopy timescales one would expect to observe a magnetic signal. If so, the muon measurements would signal magnetic behavior near the onset temperature of SMAF phase. No neutron diffraction studies have been carried out on the concentration dependence of either the SMAF or LMAF phases in  $U_{1-x}Th_xPt_3$ . However, neutron diffraction results for  $U(Pt,Pd)_3$ <sup>21</sup> show that SMAF is robust upon alloying: the transition into the SMAF state remains fixed at 6 K with increasing  $x$  (up to  $x = 0.01$ ), although the ordered moment increases with  $x$ . By analogy we expect that the SMAF phase line for  $(U,Th)Pt_3$  will be essentially independent of Th concentration and fixed at a value of approximately 6 – 7 K. Thus it would be expected that for strong disorder, one could observe magnetism beginning at about 7 K, as observed in this work. This scenario could also explain the discrepancy between recent  $\mu$ SR studies on  $UPt_3$ <sup>16,17</sup> and the much earlier work by Heffner.<sup>32</sup> In Ref. 32 a small increase in the zero-magnetic field depolarization rate was observed at the SMAF transition temperature of 6 K. However, later works on single crystals<sup>16</sup> and polycrystals<sup>17</sup> of high quality gave no evidence of the transition. It is possible that the sample quality for the work described in Ref. 32 was such that impurities played a role in slowing down the SMAF fluctuations, rendering the transition observable. At present we have no explanation as to why Th is apparently much more effective than Pd in slowing down the SMAF fluctuations.

It is difficult to test for the existence of a superconducting/antiferromagnetic mutual quantum critical point, as found for  $U(Pt,Pd)_3$ .<sup>25</sup> Apart from the  $x = 0.05$  sample, an unambiguous determination of the Néel temperature is not possible from our data. For the  $x = 0.005$  sample, it is expected that  $T_c = 0.2$  K,<sup>38</sup> while we clearly observe magnetic behavior below about 2 K. This would seem to rule out the possibility of  $x_{c,SC} \approx x_{c,AFM}$ . However, the fact that the fractional magnetic signal is about 0.6 as  $T \rightarrow 0$  K indicates that the sample may never actually exhibit fully static antiferromagnetism, and so superconductivity may coexist with a lower frequency version of SMAF.

It is also difficult to reconcile the growing body of data probing the SMAF-to-LMAF transition with the phase diagram shown in Fig. 1. Our  $\mu$ SR results imply that the transition is

not abrupt, but result from a slowing down of the SMAF oscillations. Moreover, recent studies utilizing cantilever magnetometry<sup>43</sup> with a characteristic frequency of 1 kHz do not show a magnetic transition in  $\text{U}(\text{Pt}_{0.99}\text{Pd}_{0.01})_3$  single crystals, despite what appears to be sufficient sensitivity and even though  $\mu\text{SR}$  measurements<sup>17</sup> clearly indicate a  $T_N = 1.8$  K. These results imply that SMAF-to-LMAF is not a true phase transition but rather a crossover behavior, and the details of a phase diagram such as that shown in Fig. 1 will depend on the characteristic timescale of the measuring probe, at least in some critical crossover region.

Finally we speculate on the interpretation of our results for the  $x = 0.005$  sample. We find no evidence of a static, non-zero local magnetic field (i.e.,  $\nu = 0$  in the depolarization function given in Eq. (1)), and we propose that this depolarization is caused entirely by slowed-down SMAF fluctuations. Interestingly, the amplitude associated with slow fluctuations is approximately the same as for the Kubo-Lorentz contribution to the LMAF depolarization function. This would be consistent with the interpretation of Eq. (1) as being due to approximately half the sample volume being statically ordered, while the other half has slow SMAF fluctuations, which lends further support to the idea that the LMAF phase is in fact magnetically inhomogeneous. The details of how statically ordered magnetism nucleates from the SMAF (which also has been proposed to be magnetically inhomogeneous<sup>28</sup>), will be an interesting topic for future studies.

## 5. Summary

In summary, we have used muon spin spectroscopy to study the onset of the large-moment antiferromagnetic phase (LMAF) in  $\text{UPt}_3$  as induced by Th-substitution. We find that the two-component response function used to characterize the muon response in Pd-induced LMAF is also applicable to  $(\text{U,Th})\text{Pt}_3$ . However, the transition into the antiferromagnetic phase as temperature is lowered is much broader for Th substitution than for Pd substitution. While this broad transition makes it difficult to detail the competition between superconductivity and LMAF in  $(\text{U,Th})\text{Pt}_3$ , it may be a result of the effects of disorder of the time fluctuations associated with an anomalous antiferromagnetic state (SMAF). These results imply that SMAF-to-LMAF is not a true phase transition but rather a crossover behavior. We are currently conducting detailed materials analysis and thermodynamic studies to test for this possibility.

We thank Eric J. Peterson of Los Alamos National Laboratory for carrying out x-ray diffraction measurements on the samples used in this study. This work was supported by the

Petroleum Research Fund of the American Chemical Society, DOE grant DEF 60202ER63404, the FERLIN program of the European Physical Society, the European Science Foundation, and at Los Alamos it was performed under the auspices of the U.S.D.O.E.

## References

- [1] See J. A. Sauls, *Adv. Phys.* **43**, 113 (1994).
- [2] G. Aeppli *et al.*, *Phys. Rev. Lett.* **60**, 615 (1988)
- [3] R. A. Fisher *et al.*, *Phys. Rev. Lett.* **62**, 1411 (1989)
- [4] G. Bruls *et al.*, *Phys. Rev. Lett.* **65**, 2294 (1990); S. Adenwalla *et al.*, *Phys. Rev. Lett.* **65**, 2298 (1990).
- [5] G. Aeppli *et al.*, *Phys. Rev. Lett.* **63**, 676 (1989).
- [6] E. D. Isaacs *et al.*, *Phys. Rev. Lett.* **75**, 1178 (1995).
- [7] H. Tou *et al.*, *Phys. Rev. Lett.* **80**, 3129 (1998)
- [8] Y. Dalichaouch *et al.*, *Phys. Rev. Lett.* **75**, 3938 (1995).
- [9] H. G. M. Duijn *et al.*, *Physica B* **223&224**, 44 (1996).
- [10] S. M. Hayden *et al.*, *Phys. Rev. B* **46**, 8675 (1992).
- [11] R. J. Keizer *et al.*, *Physical Review B* **60**, 10527 (1999).
- [12] M. C. Aronson *et al.*, *Physica B* **186-188**, 788 (1993).
- [13] P. A. Midgley *et al.*, *Phys. Rev. Lett.* **70**, 678 (1993).
- [14] D. A. Walko *et al.*, *Phys. Rev. B* **63**, 054522 (2001).
- [15] H. Tou *et al.*, *Phys. Rev. Lett.* **77**, 1374 (1996).
- [16] P. Dalmas de Réotier *et al.*, *Phys. Lett. A* **205**, 239 (1995).
- [17] R. J. Keizer *et al.*, *J. Phys.: Condens. Matter* **11** 8591 (1999).
- [18] Y. Okuno and K. Miyake, *J. Phys. Soc. Jap.* **67**, 3342 (1998).
- [19] Y. Sidis *et al.*, *Phys. Rev. Lett.* **86**, 4100 (2001)
- [20] P. Frings, B. Renker, and C. Vettier, *J. Magn. Magn. Mat.* **63&64**, 202 (1987).
- [21] R. J. Keizer *et al.*, *Phys. Rev. B* **60**, 6668 (1999).
- [22] Y. Kohori and T. Kohara, *Physica B* **284-288**, 1283 (2000).
- [23] A. de Visser *et al.*, *J. Magn. Magn. Mater.* **54-57**, 375 (1986).
- [24] G. R. Stewart *et al.*, *Phys. Rev. B* **34**, 4629 (1986).
- [25] A. de Visser *et al.*, *Phys. Rev. Lett.* **85**, 3005 (2000).
- [26] Ziqiang Wang, Wenjin Mao, and Kevin Bedell, *Phys. Rev. Lett.* **87**, 257001 (2001)
- [27] See for example A. Amato, *Rev. Mod. Phys.* **69**, 1119 (1997).
- [28] A. Yaouanc *et al.*, *Phys. Rev. Lett.* **84**, 2702 (2000).

- [29] A. Schenck *et al.*, Physica B **289-290**, 455 (2000).
- [30] K. Matsuda *et al.*, Phys. Rev. Lett. **87**, 087203-1 (2000)
- [31] A. I. Goldman *et al.*, Phys. Rev. B **34**, 6564 (1986).
- [32] R. H. Heffner *et al.*, Phys. Rev. B **39**, 11345 (1989).
- [33] A. P. Ramirez, B. Batlogg, E. Bucher, and A. S. Cooper, Phys. Rev. Lett. **57**, 1072 (1986).
- [34] B. Batlogg, *et al.*, J. Magn. Magn. Mater. **63&64**, 441 (1987).
- [35] C. P. Opeil and M. J. Graf, Physica B **319**, 246 (2002)
- [36] W. Trinkl, S. Corsépius, and G. R. Stewart, J. Alloys Compounds **240**, 96 (1996).
- [37] M. J. Graf, R. J. Keizer, A. de Visser, and S. T. Hannahs, Physica B **284-288**, 1281 (2000).
- [38] T. Vorenkamp *et al.*, Phys. Rev. B **48**, 6373 (1993).
- [39] C. Domb, *The Critical Point* (Taylor and Francis, London, 1996)
- [40] R. Kubo, Phys. Rev. **87**, 568 (1952).
- [41] K. Kadowaki *et al.*, Physica **148B**, 22 (1987).
- [42] It should be noted that the expected changes in  $c/a$  induced by a small amount of Pd or Th substitution are extrapolated from values measured at higher concentrations, since the changes are quite small and difficult to measure through x-ray analysis.
- [43] C. P. Opeil, A. de Visser, M. J. Naughton, and M. J. Graf, submitted for publication.

## FIGURE CAPTIONS

Fig. 1 The superconducting and magnetic phase diagram of  $U(\text{Pt}_{1-x}\text{Pd}_x)_3$ , adapted from Ref. 22.

Fig. 2 Variation of the residual resistivity with Th concentration for the samples studied in this work. The two values for  $x = 0.02$  are for independently fabricated samples. The solid line is a guide to the eye.

Fig. 3 The short-time depolarization as a function of time for several  $U_{1-x}\text{Th}_x\text{Pt}_3$  samples taken at low-temperature ( $T = 1.8$  K). Solid lines represent the fits to the data using Eq. (1).

Fig. 4 Variation of the fitting parameters for Eq. (1) with concentration, evaluated at  $T = 1.8$  K for all concentrations except  $x = 0.006$ , which was evaluated at 100 mK. Filled symbols are for  $U_{1-x}\text{Th}_x\text{Pt}_3$ . For comparison we show similar results for  $U(\text{Pt}_{1-x}\text{Pd}_x)_3$  (open symbols) taken from Ref. 17.

Fig. 5 Variation of the ratio of the oscillatory component to the Kubo-Lorentz component (see Eq. (1)) with Th concentration.

Fig. 6 Temperature dependence of the spontaneous oscillation frequency for  $U_{0.95}\text{Th}_{0.05}\text{Pt}_3$  and  $U_{0.98}\text{Th}_{0.02}\text{Pt}_3$ . The solid lines are the mean-field fits for  $x = 0.05$  and  $x = 0.02$ , as described in the text. The squares and triangles for the  $x = 0.02$  denote results for two independently fabricated samples.

Fig. 7 Temperature dependence of the Kubo-Lorentz damping factor for  $U_{0.95}\text{Th}_{0.05}\text{Pt}_3$  and  $U_{0.98}\text{Th}_{0.02}\text{Pt}_3$ . The solid line is a mean-field type fit for  $x = 0.05$ , as described in the text. The squares and triangles for the  $x = 0.02$  denote results for two independently fabricated samples.

Fig. 8 Temperature evolution of the depolarization function at short times for  $U_{0.98}\text{Th}_{0.02}\text{Pt}_3$ . Note that all temperatures are above the mean-field Néel temperature of 5.05 K.

Fig. 9 Transition widths as illustrated by the temperature-dependent fractional amplitude associated with magnetism. Circles are for  $U_{1-x}\text{Th}_x\text{Pt}_3$  while triangles are for  $U(\text{Pt}_{1-x}\text{Pd}_x)_3$  with equivalent  $x$  values, taken from the work of Ref. 17. Solid and dashed lines are guides to the eye for the Th-substituted and Pd-substituted data, respectively.

Fig. 10 Temperature dependence of the fraction of total amplitude of the depolarization function associated with magnetic behavior for  $U_{0.995}\text{Th}_{0.005}\text{Pt}_3$ .

Figure 1

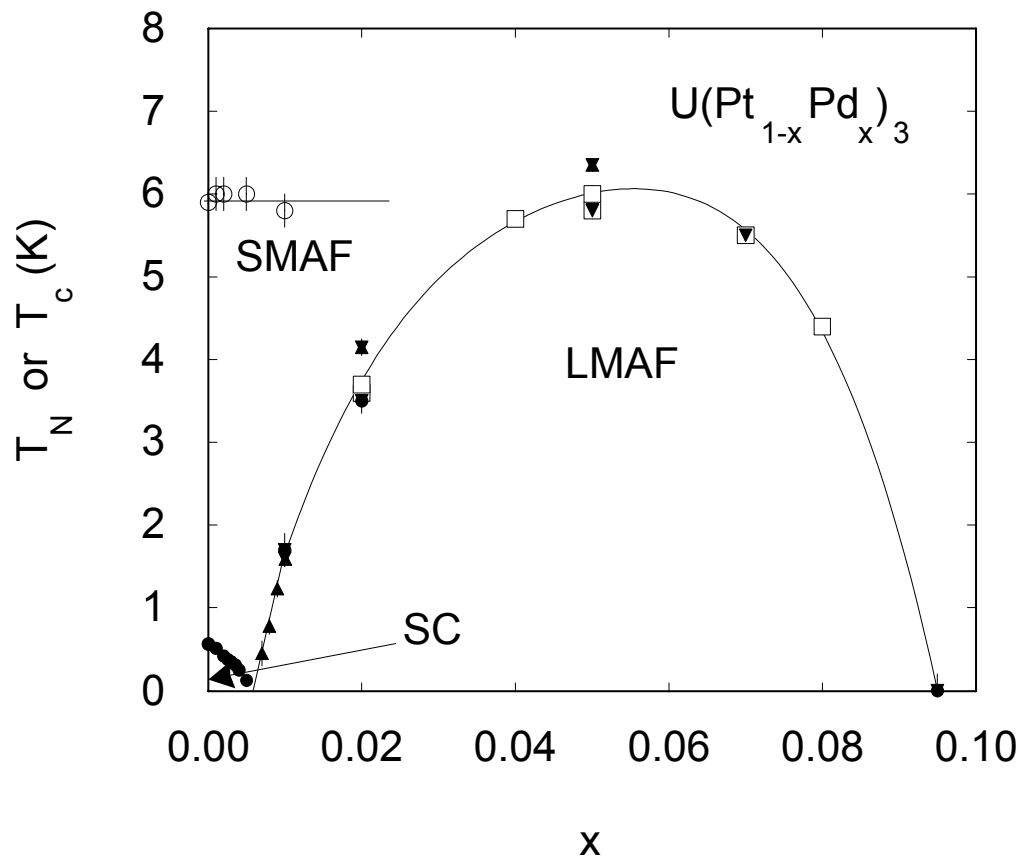


Figure 2

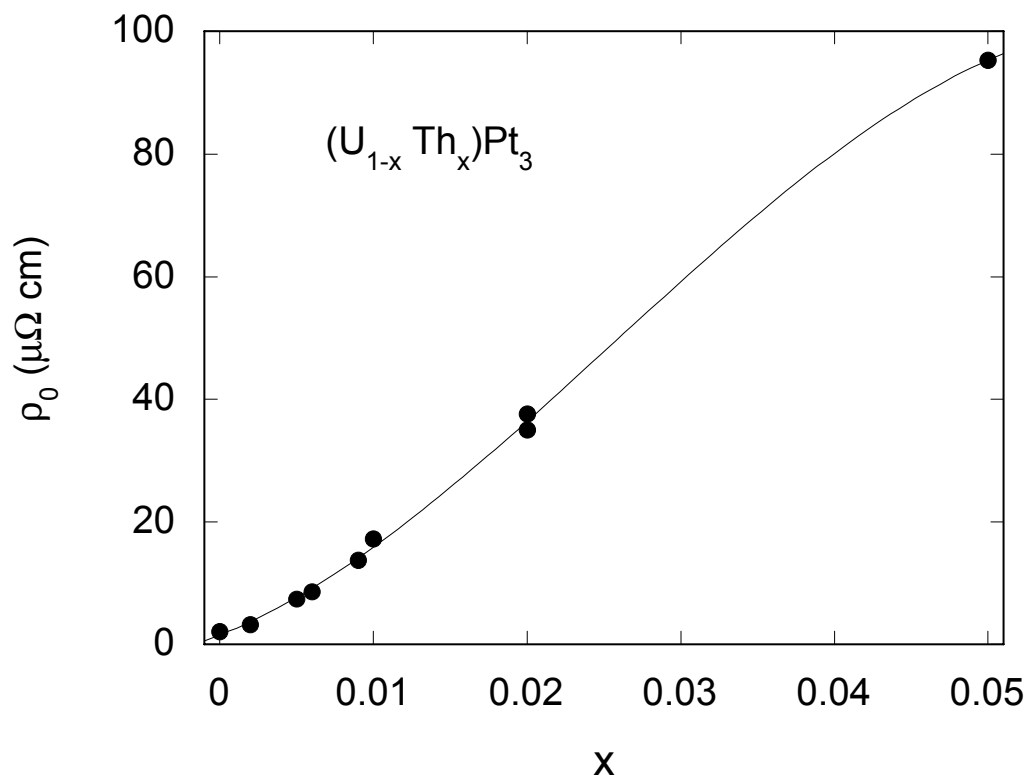


Figure 3

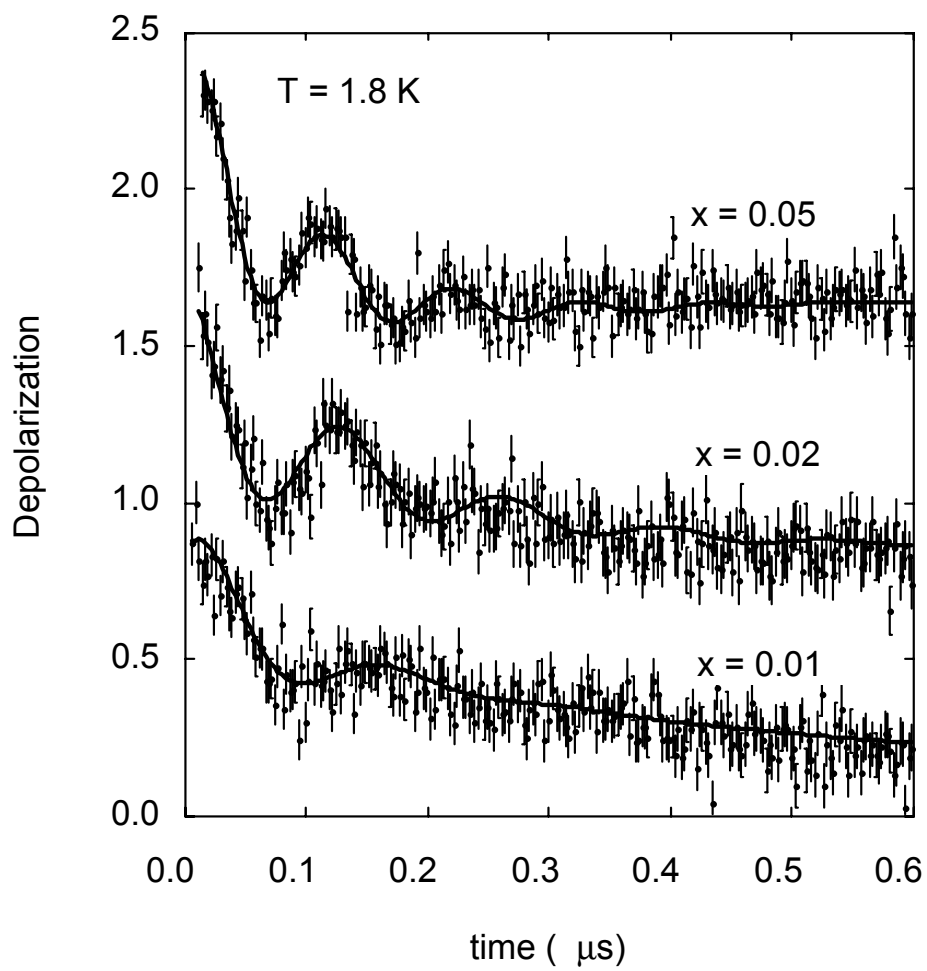


Figure 4

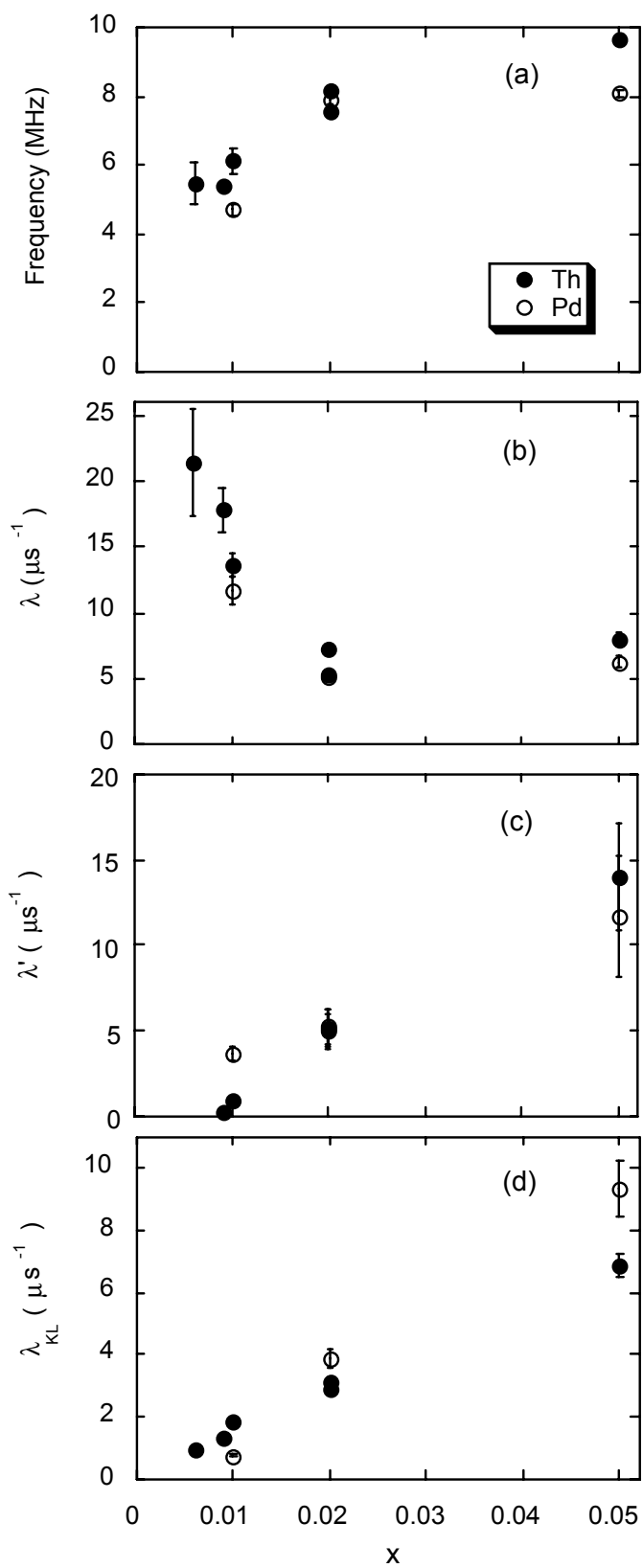


Figure 5

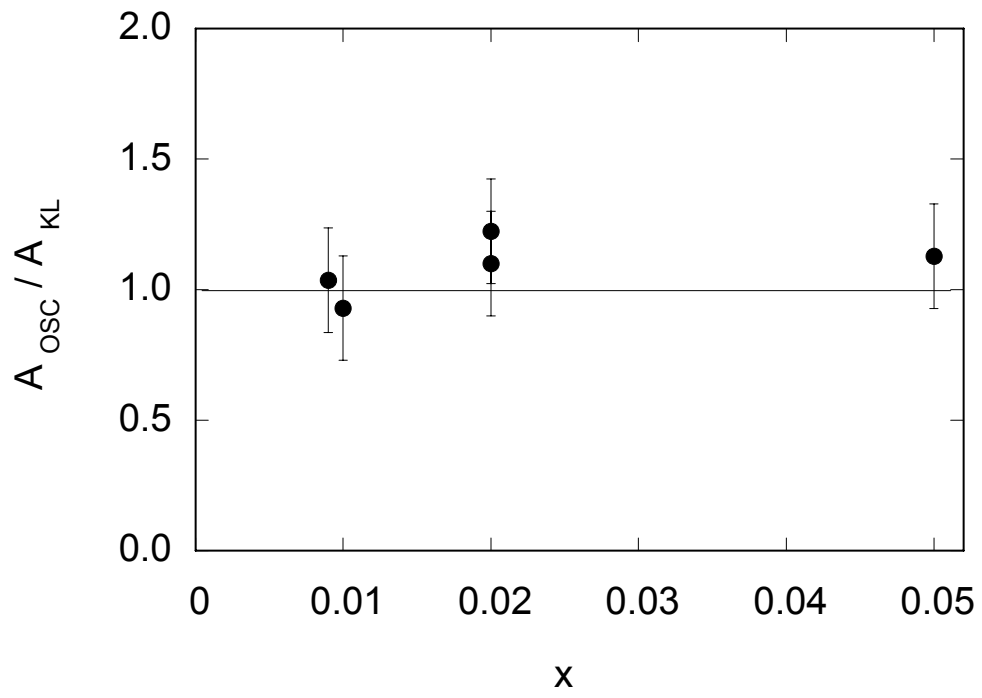


Figure 6

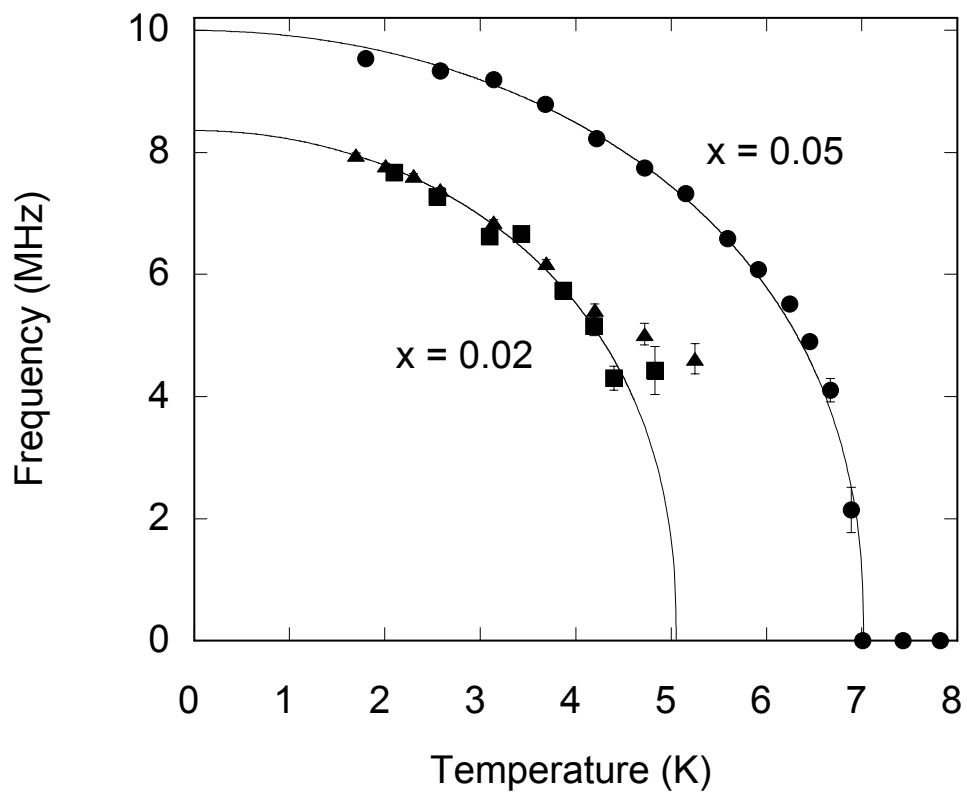


Figure 7

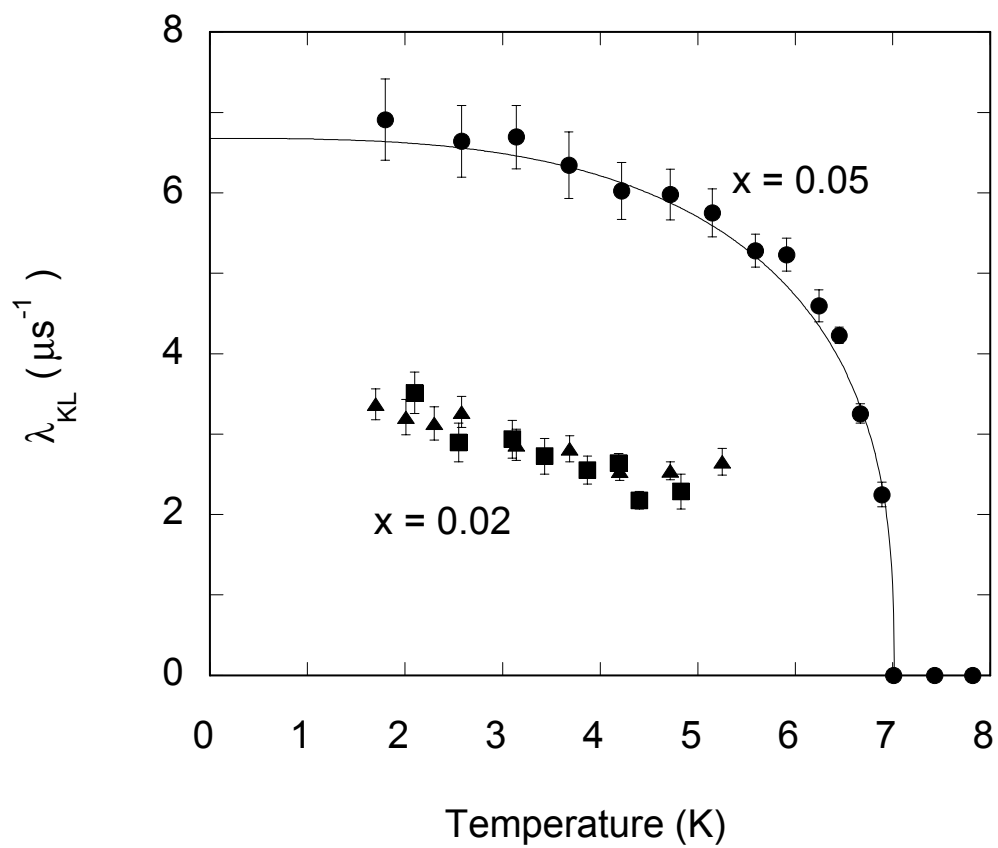


Figure 8

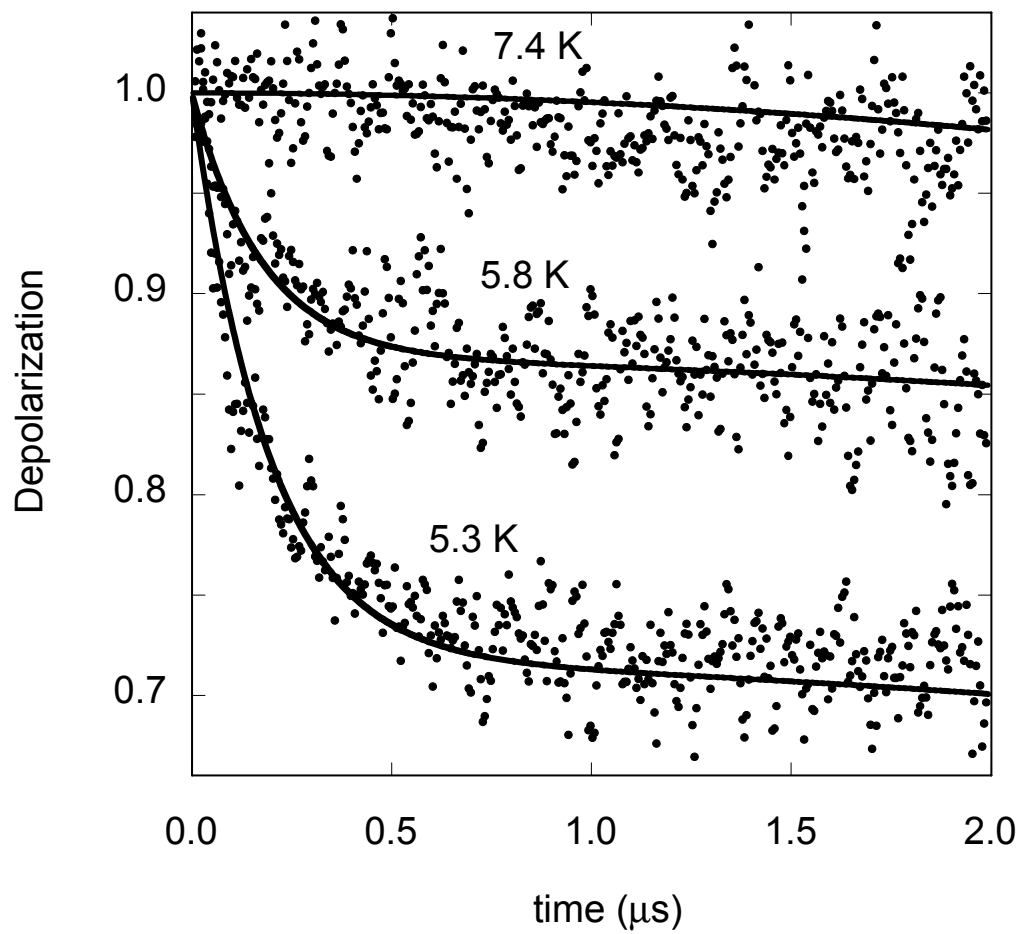


Figure 9

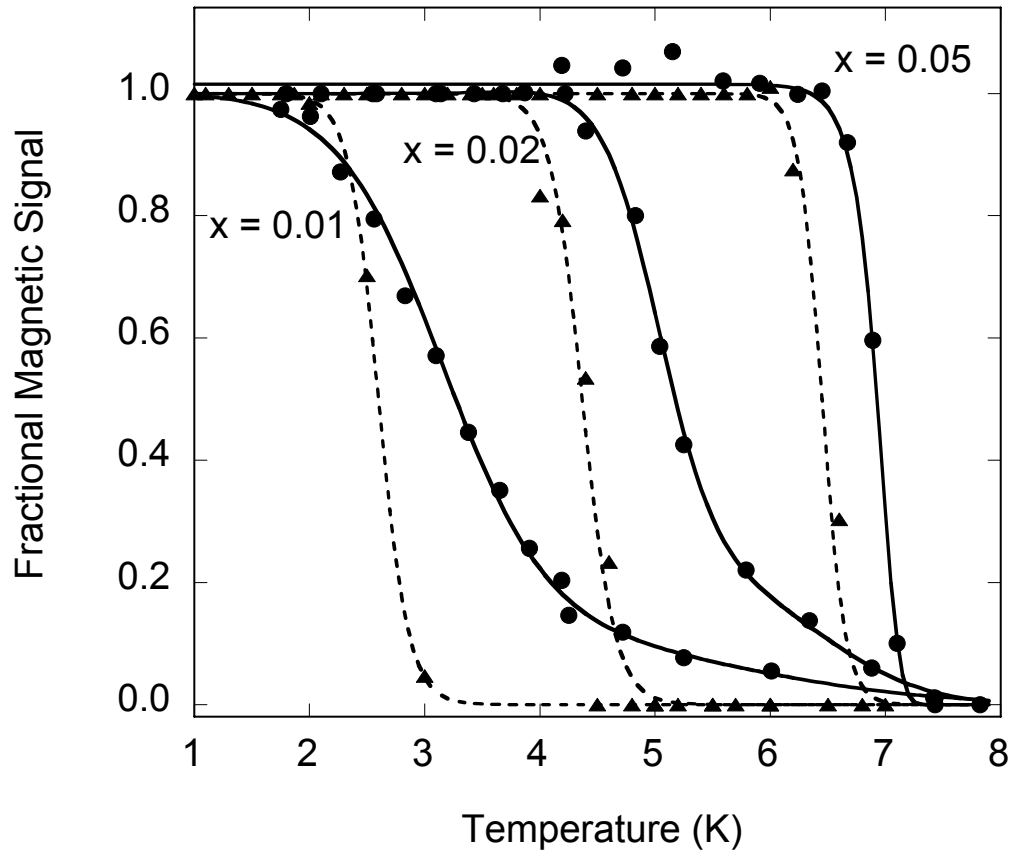


Figure 10

